Aromaticity and Chemical Bonding of Chalcogen-Bonded Capsules Featuring Enhanced Magnetic Anisotropy

Demeter Tzeli,*[a, b] Ioannis D. Petsalakis,*[b] Giannoula Theodorakopoulos,[b] Faiz-Ur Rahman,[c] Pablo Ballester,[d, e] Julius Rebek, Jr.,[c, f] and Yang Yu[c]

We present a theoretical study of chalcogen bonded container capsules ($\mathbf{A_X}+\mathbf{A_X}$) where X=O, S, Se, and Te, and their encapsulation complexes with *n*-C_9H_{20} (*n*-C_9H_{20}@$\mathbf{A_X}+\mathbf{A_X}$). Both Se and Te encapsulation complexes have significant experimental and computed binding energies, analogous to the hydrogen bonded counterparts, while the S and O capsules and their encapsulation complexes show only weak binding energies, which are attributed to different types of bonding: chalcogen S···N bonds for S-capsules and π–π stacking and weak hydrogen bonds for the O case. All $\mathbf{A_X}+\mathbf{A_X}$ and C_9H_{20}@$\mathbf{A_X}+\mathbf{A_X}$ present unusually high magnetic anisotropies in their interiors. The ^{1}H NMR spectra of the encapsulation complexes display the proton signals of the encapsulated *n*-nonane highly upfield shifted, in agreement with the available experimental data for the Se capsule. We found that different factors contribute to the observed magnetic anisotropy of the capsule's interior: for the Te capsule the most important factor is Te's large polarizability; for the O analogue the inductive effects produced by the electronegative nature of the O and N heteroatoms; and for the S and Se capsules, the polarizability of the heteroatoms combines with electric field effects.

1. Introduction

We recently described a new water-soluble capsule that assembles through dimerization of cavitands mediated by chalcogen bonding involving Se atoms.[1] The cavitand hemispheres of the capsule feature four 3,1,2 benzo selenodiazole panels (Figure 1 and Scheme 1) displaying Se and N atoms in a self-complementary array appropriate for chalcogen bonding. Previously, Diederich[2] introduced structurally related capsules soluble in organic solvents that were assembled by chalcogen bonding mediated by S and Te atoms. Remarkably, the Se capsule showed reversible encapsulation in aqueous solution. Encapsulation studies involving a series of guests were analyzed using ^{1}H NMR spectroscopy. The obtained results revealed an unexpected feature of the chalcogen-bonded Se capsule compared to hydrogen-bonded analogues: the magnetic environment of the former caused larger upfield shifts for the guest nuclei, particularly near the center of the capsule, than in the latter. Preliminary calculations suggested an enhanced aromaticity near the Se atoms. Because reactions inside related containers have been shown to respond to peripheral charac-

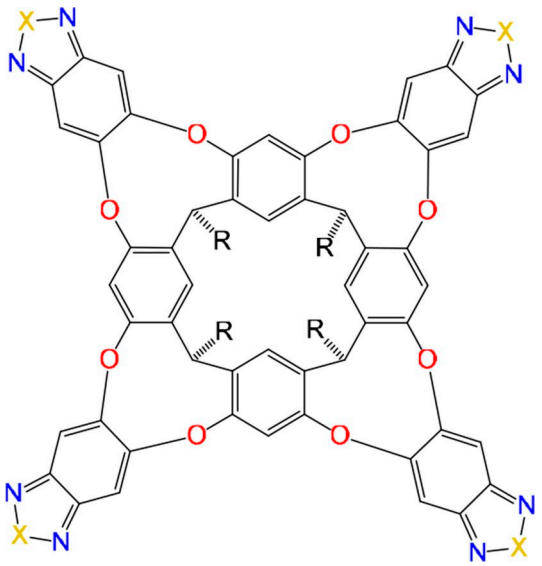

Scheme 1. Line drawing structure of the A_x cavitands equipped with four 3,1,2 benzo X-diazole panels. (R = *n*-C_3H_6Cl, X(Chalcogen) = O, S, Se, and Te.

[a] *Prof. D. Tzeli*
Laboratory of Physical Chemistry
Department of Chemistry
National and Kapodistrian University of Athens
Panepistimiopolis Zografou, Athens 157 84 (Greece)
E-mail: tzeli@chem.uoa.gr
[b] *Prof. D. Tzeli, Dr. I. D. Petsalakis, Dr. G. Theodorakopoulos*
Theoretical and Physical Chemistry Institute
National Hellenic Research Foundation
48 Vassileos Constantinou Ave., Athens 116 35 (Greece)
E-mail: idpet@eie.gr
tzeli@chem.uoa.gr
[c] *Dr. F.-U. Rahman, Prof. J. Rebek, Jr., Prof. Y. Yu*
Center for Supramolecular Chemistry &
Catalysis and Department of Chemistry
College of Science, Shanghai University
Shanghai 200444 (China)
[d] *Prof. P. Ballester*
Institute of Chemical Research of Catalonia (ICIQ)
43007 Tarragona (Spain)
[e] *Prof. P. Ballester*
Catalan Institution for Research and Advanced Studies (ICREA)
08010 Barcelona (Spain)
[f] *Prof. J. Rebek, Jr.*
Skaggs Institute for Chemical Biology and Department of Chemistry
The Scripps Research Institute
La Jolla, California 92037 (United States)

Supporting information for this article is available on the WWW under https://doi.org/10.1002/cphc.202000654

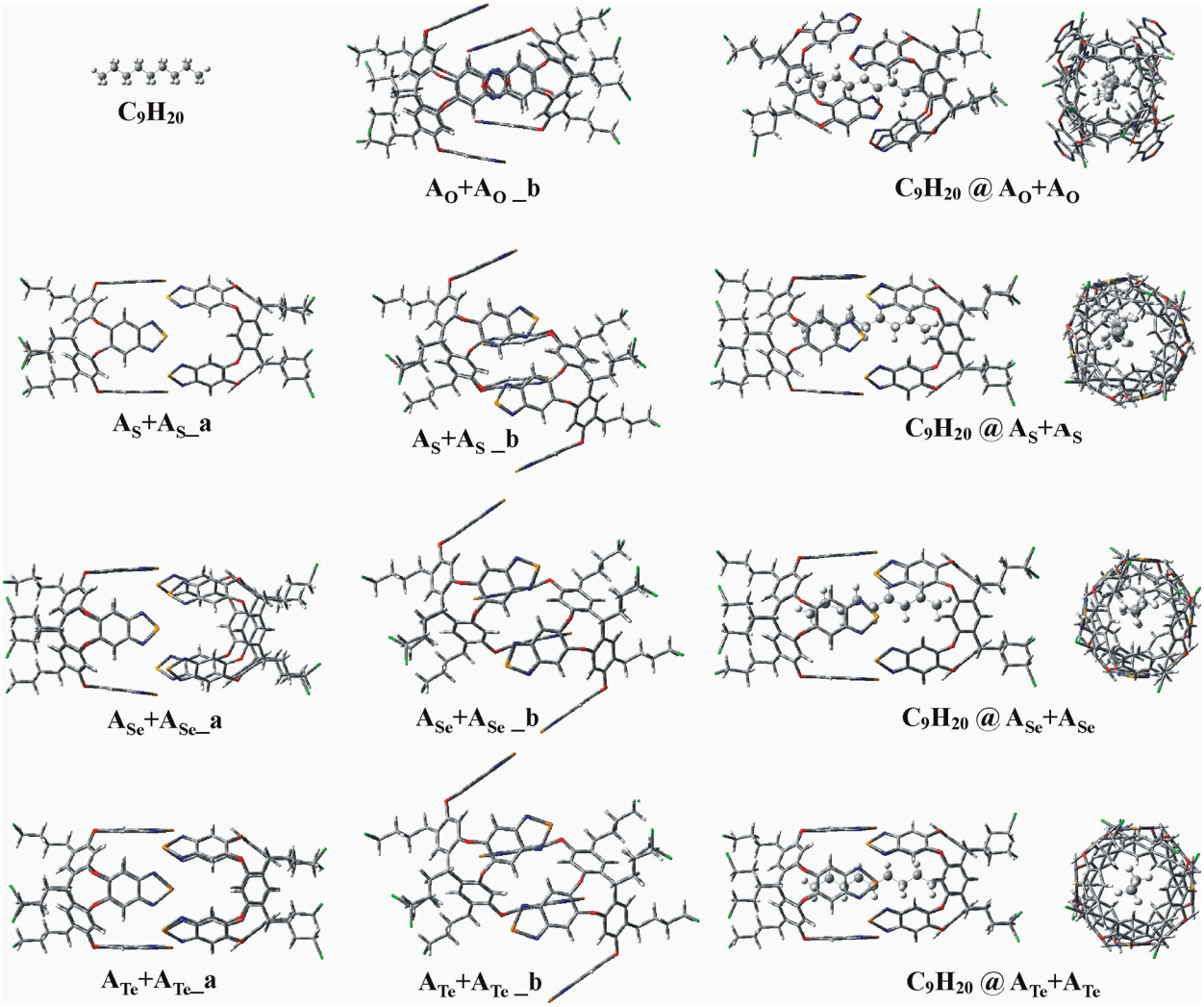

Figure 1. Calculated capsules, $A_X + A_X$ and encapsulated complexes $C_9H_{20}@A_X + A_X$.

teristics such as charge[3–5] and Bronsted acidity,[6] we were curious to explore the origin and nature of the anisotropic magnetic environment of the capsule's interior. While O is usually not considered a chalcogen bond acceptor, it is of interest to examine this possibility in the assembly of the capsules. Recently, experimental evidence of chalcogen bonding of O atoms as acceptor unit has been described.

We began by examining the details of the cohesive force for capsule formation, the chalcogen bond. Typically, chalcogen bonding occurs between the electron deficient Group VI elements (S, Se, Te) and nucleophile sites i.e., electron donor species. Dimeric benzoselenadiazoles, and benzotelluradiazoles have been well-studied.[7–10] It has been found that the strongest chalcogen-bonding interactions are at least as strong as the conventional H-bonds, but unlike H-bonds, they are surprisingly not solvent dependent.[11] Te forms the strongest chalcogen bonding interactions compared to the other chalcogens, which can reach up to 7 kcal/mol.[12] Regarding the chalcogen-N bonding, although there is an important electrostatic component, the interaction is interpreted as the donation of a nitrogen lone pair into the chalcogen-centered anti-bonding orbitals.[13]

As mentioned above, O is not considered to be a chalcogen bond acceptor. The heavier chalcogen atoms (S, Se, and Te) form chalcogen bonds because the electron cloud of the chalcogen atom can be modified by an electron withdrawing substituent producing an electrophilic s-hole.[14] It is known that O forms chalcogen O…S and O···O bonding interactions.[15] However, in the latter case only when highly activated oxygen acceptor atoms are involved.[14] For this reason, we were interested in examining the possibility of the formation of analogous dimeric capsules with O atoms.

In the present study, we use Density Functional Theory (DFT) calculations to study the chalcogen bonding of four chalcogen atoms with nitrogen atoms, i.e., N···X bonding (X=O, S, Se, and Te) occurring in the dimerization of $\mathbf{A_X}$ cavitands, see Scheme 1, leading to the $\mathbf{A_X + A_X}$ capsules, see Figure 1. We determined the binding energies of the two cavitands and the encapsulation energies of nonane, *n*-C_9H_{20}, as guest of these capsules. Additionally, the bonding energies were analyzed in

many-body interaction energy terms. Regarding the unusually high magnetic anisotropy observed experimentally for the interior of the $\mathbf{A_{Se}+A_{Se}}$ capsule,[1] we became interested in examining whether analogous phenomena occurred in the other (X=O, Te, and S) $\mathbf{A_X+A_X}$ capsules. In an effort to reveal the factors leading to the increased magnetic anisotropy, we calculated dipole moments, dipole electric field, isotropic and anisotropic polarizabilities, and NMR spectra. We also produced contour plots of magnetic isotropy and anisotropy, as well as NICS aromaticity indexes of the capsules ($\mathbf{A_X+A_X}$) and of their encapsulated complexes with *n*-C_9H_{20} as guest. Note that, NICS indexes are widely used to characterize aromaticity and antiaromaticity of ring systems, see below.

2. Methodology

The chalcogen-bonded $\mathbf{A_X+A_X}$ capsules (X=O, S, Se and Te), as well as their encapsulated complexes with *n*-C_9H_{20} were geometry optimized at the M06-2X[16]/ LANL2DZ[17] level of theory. Single-point calculations of the energy-minimized capsules were also carried out at the M06-2X/6-31G(d,p),[18] PBE0[19]/LANL2DZ, and PBE0/6-31G(d,p) levels of theory. We use two functionals and two basis sets in order to check our data regarding the geometries and properties. Previous studies on encapsulations studies showed that the M06-2X/6-31G(d,p) methodology was appropriate and provided similar results to the M06-2X/6-311+G(d,p) methodology, where a larger basis set is employed.[20] Additionally, the properties of part of the walls of the capsules, cf. furazan (**1**) and its substituted derivatives with S (**2**), Se (**3**) and Te atoms (**4**), see Figure 1S of SI, were calculated at the DFT level with a series of functionals and basis set, as well as at the MP2 and CCSD levels in order to compare the obtained results see SI. We found that the DFT level calculate adequately the properties of the assemblies and the M06-2X/6-31G(d,p) methodology was our best choice.

The binding energies of the $\mathbf{A_X+A_X}$, as well as the binding energies of their encapsulated complexes with *n*-C_9H_{20} were also calculated at different levels of theory. In all interaction energies and dimerization energies presented here, the basis set superposition error (BSSE) corrections have been taken into account using the counterpoise procedure.[21] An analysis of the many-body interaction energy terms was performed[22] corrected for the BSSE;[23] the terms, i.e., 2-body, 3-body and deformation (D), are given in the supporting information (SI). This analysis offers insights into the added stabilization of the 3-body system, i.e., 2 cavitands + guest while information is also obtained on the possible distortion required for the formation of the encapsulated complexes. Additionally, dipole moments, dipole electric field isotropic and anisotropic polarizabilities, ^{1}H and ^{13}C NMR spectra, contour plots of magnetic isotropy and anisotropy in the whole cavity, were calculated at all levels of theory. NMR shielding tensors have been computed with the Gauge-Independent Atomic Orbital (GIAO) method.[24] Finally, the Nucleus-Independent Chemical Shifts (NICS) were computed and used as aromaticity indexes.[25] All calculations were carried out with the aid of the Gaussian16 program.[26]

3. Results and Discussion

3.1. Geometries and Binding Energies

The calculated capsules, $\mathbf{A_X+A_X}$ and their encapsulated complexes with the C_9H_{20} alkane, $\mathbf{C_9H_{20}@A_X+A_X}$ are depicted in Figure1. In the case of the $\mathbf{A_X+A_X}$ capsules, two minimum energy structures were determined. In the first one, $\mathbf{A_X+A_X\_a}$, the two cavitands face each other, forming sixteen N···X bonds, see Figure 2, while in the second, $\mathbf{A_X+A_X\_b}$, one cavitand goes inside the other forming π–π stacking bonds, which are parallel-displaced, and CH···N bonds, see Figure 2. In the case of **_b** structures, eight π–π stacking bonds and eight CH···N bonds are formed for the O capsule, while three π–π stacking bonds and twelve CH···N bonds are formed for the remaining chalcogens, see close-up structures in Figure 2. It should be noted that in the case of the oxygen derivative, $\mathbf{A_O+A_O}$, only the $\mathbf{A_X+A_X\_b}$ structure is calculated as stable, because N···O bonds are not formed. This result is in striking contrast with our findings for the N···X bonds present in the dimeric assemblies of the other chalcogen atoms. It is also notable that the chalcogen atoms, except for O, are positively charged, while the charge of

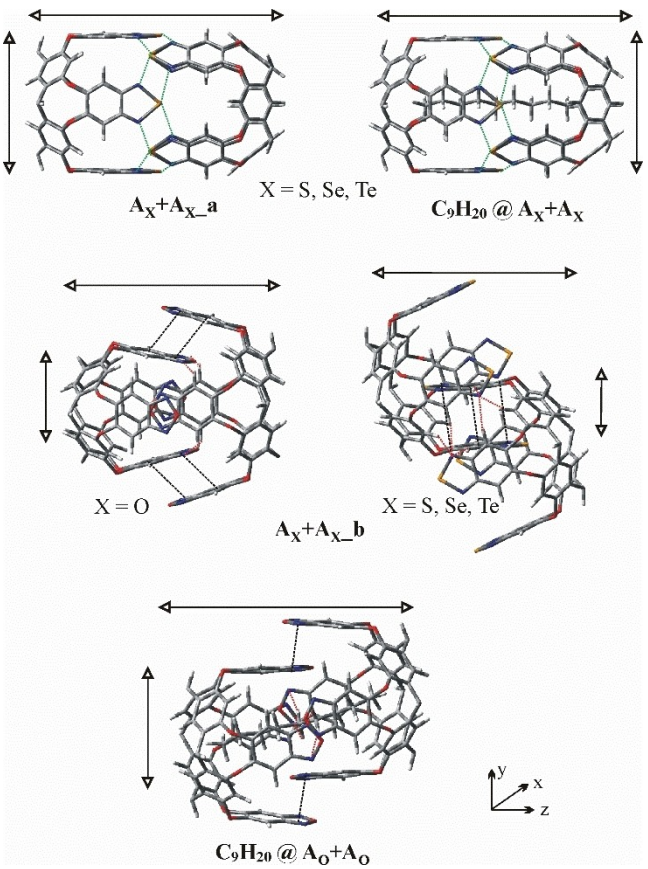

Figure 2. Close up structures of the $A_X+A_X\_a$ and $A_X+A_X\_b$ capsules and of the $C_9H_{20}@A_X+A_X$ (X=S, Se and Te) and $C_9H_{20}@A_O+A_O$ complexes (cf. Figure 1), where the X···N interactions (green dotted lines), the π–π stacking interactions (black dotted lines) and CH···N hydrogen bonds (red dotted lines) are shown. For reason of clarity not all of the π–π stacking CH···N hydrogen bond interactions are indicated.

the O atom is almost zero. On the other hand, the N atoms are negatively charged in all cases, see below. As shown in Figure 1, the encapsulated complexes, $\mathbf{C_9H_{20}@A_X+A_X}$ involve the **_a** form for X=S, Se, Te and an elongated **_b** form for X=O (see also Figure 2).

In relation to the size of the capsules, see Table 1, all $\mathbf{A_X+A_X\_a}$ are identical (16.7 Å). Likewise, all $\mathbf{A_X+A_X\_b}$ display similar lengths of the order of 13.2 Å. However, the cavity volumes of the capsules are different, because the established π–π stacking interactions and CH···N bonds are dissimilar, see Figure 2. Sixteen N···X intermolecular bonds are formed in $\mathbf{A_X+A_X\_a}$ isomeric capsules and their encapsulation complexes $C_9H_{20}@\mathbf{A_X+A_X}$. The distances of the chalcogen bonds are in the range of 2.5 to 3.2 Å, see Table 1. These distances are in agreement with those observed in single-crystal X-ray structures for the case of S,[2] Se[1] and Te[2] including guests, i.e., two methylbenzene molecules for S-, *n-nonane* for Se-, and two benzene for Te-capsule.

As mentioned above, in the case of the oxygen-based capsule only the $\mathbf{A_O+A_O\_b}$ structure is stable. When the alkane is encapsulated, i.e., $C_9H_{20}@\mathbf{A_O+A_O}$, the capsule elongates and the eight π–π stacking interactions stabilizing the dimer (see above) are not observed. However, four new π–π interactions are formed in the encapsulation complex, as well as additional CH···N and CH···O bonds between encapsulated *n*-nonane and the aromatic walls of the O-cavitands, see Figure 2. In all $\mathbf{A_X+A_X\_b}$ structures, the N···HC bond distances range from 2.2 (S) to 2.8 (O and Te) Å, while the π–π stacking interactions distances are 3.3 Å (O) and 3.6 Å (S). In the cases of Se and Te, the π–π stacking interactions are very weak, and their distances are about 4.2 Å. Energetically favorable π–π stacking interaction distances are in the range of 3.3 −3.8 Å[27] length and their energies are close to 0.1 eV (2–3 kcal/mol).[28]

The binding energies of the more stable capsules are −1.4(O) −1.5(S) eV and −1.8(S) and −4.6 eV (Te), see Table 1. In the cases of the S and Se atoms, the **a** and **b** structures of the $\mathbf{A_X+A_X}$ capsules are almost degenerate in energy. Nevertheless, this is not the case for the Te capsule. The energetic price paid for the non-coplanar array is large for Te, i.e., 2.5 eV and small for Se 0.2 eV. On the other hand, for S, the **b** structure is 0.1 eV lower in energy, that is, the non-coplanar array is slightly more stable. This means that in the case of S, the energy gain from the formation of N···X bonds (chalcogen bonds) is almost the same than the energy gained from π–π stacking interactions and CH···N bonds.

The binding energies of $C_9H_{20}@\mathbf{A_X+A_X}$ encapsulation complexes with respect to the three free components (ΔE_1) and with respect to the empty capsule and the free alkane, (ΔE_2), as the chalcogen atom changes from O to Te, are listed in Table 1. We observe that the ΔE_1 values increase with the size of the chalcogen's atom. For Te a significantly large binding energy of −5.3 eV is calculated. The ΔE_2 values are small, less than 1 eV in magnitude. The O based capsule presents the smallest binding energy, i.e., −0.2 eV. However, despite this small binding energy, the $C_9H_{20}@\mathbf{A_O+A_O}$ complex is a stable (minimum energy) structure.

The ΔE_1 and ΔE_2 energy values of the capsules and encapsulated complexes were analyzed in the many-body interaction energy terms, i.e., 2-body, 3-body and deformation (D), see Figure 3. We observe that comparing the $\mathbf{A_X+A_X\_a}$ and $\mathbf{A_X+A_X\_b}$ structures, the deformation of the cavitands is larger in the **a** structures. In other words, the formation of the chalcogen bonding distort the structures of the bonded $\mathbf{A_X}$ with respect to that in the free $\mathbf{A_X}$. However, the gain in the 2B term is larger in **a** structures for both Se and Te capsules. The deformation energies of the encapsulation complexes $C_9H_{20}@\mathbf{A_X+A_X}$ and the empty dimers $\mathbf{A_X+A_X\_a}$ (X=S–Te) are the same. This result demonstrates that the encapsulation of the alkane does not significantly alter the geometry of the capsules. However, for the O capsule, the deformation energy experienced by the encapsulation complex is large, cf., 0.94 eV because the $\mathbf{A_O+A_O\_b}$ structure needs to be severely distorted to allow the encapsulation of the alkane. More bonds need to be broken in order to allow the alkane to be encapsulated and thus the encapsulation is more difficult than in the other cases. Finally, it is worth noting that the 3B term is negative, i.e., the interaction of the three components in the $C_9H_{20}@\mathbf{A_X+A_X}$ further stabilizes the encapsulated complexes.

Table 1. Size of the calculated capsules[a] and encapsulated complexes and interaction bond distances in [Å]. Binding energies ΔE_1[b] and ΔE_2[c] in [eV], at M06-2X/6-31G(d.p). Experimental values are given in parenthesis.

Capsule	Size[a]	CH···N	π–π	N…X	ΔE_1[b]	ΔE_2[c]
$\mathbf{A_S+A_S\_a}$	9.8×9.8×16.8			2.95	−1.38	
$\mathbf{A_{Se}+A_{Se}\_a}$	9.4×10.1×16.7			2.9–3.2(2.94–3.04)[d]	−1.80	
$\mathbf{A_{Te}+A_{Te}\_a}$	9.8×9.8×16.8			2.5–2.8	−4.58	
$\mathbf{A_O+A_O\_b}$	6.0×6.0×13.3	2.8	3.3		−1.36	
$\mathbf{A_S+A_S\_b}$	3.8×10.4×13.1	2.2–2.4	3.6		−1.48	
$\mathbf{A_{Se}+A_{Se}\_b}$	4.1×10.1×13.2	2.3–2.6	4.1		−1.63	
$\mathbf{A_{Te}+A_{Te}\_b}$	3.8×10.4×13.1	2.3–2.6	4.3		−2.09	
$C_9H_{20}@\mathbf{A_O+A_O}$	7.0×7.9×14.4	2.6–2.8	3.2	3.0–3.2	−1.85	−0.23
$C_9H_{20}@\mathbf{A_S+A_S}$	9.5×10.1×16.8			2.95(3.0–3.5)[e]	−2.30	−0.93
$C_9H_{20}@\mathbf{A_{Se}+A_{Se}}$	9.2×10.3×16.6			2.8	−2.67	−0.94
$C_9H_{20}@\mathbf{A_{Te}+A_{Te}}$	9.5×10.1×16.8			2.6–2.7(2.6–2.9)[f]	−5.33	−0.87

[a] See Figure 2. [b] With respect to the cavitands + alkane. [c] With respect to the capsule + alkane. [d] Single-crystal X-ray structure; Ref. [1]. [e] X-ray crystal structure, but including two methylbenzene molecules; Ref. [2]. [f] X-ray crystal structure including two benzene molecules; Ref. [2].

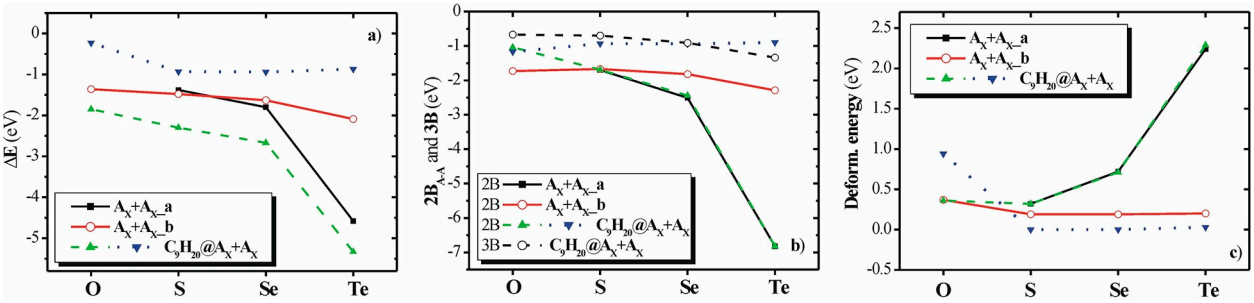

Figure 3. a) BSSE corrected dissociation energy, ΔE; b) 2-body term with respect to the two cavitands, 2B; c) Deformation energy of the $A_X + A_X$ and C_9H_{20}@A_X + A_X molecules at the M06-2X/6-31G(d.p) level of theory. Green dash lines with respect to the three species of C_9H_{20}@$A_X + A_X$, blue dot lines with respect to C_9H_{20} and the capsule $A_X + A_X$.

3.2. Properties

The results of the calculations of the capsules and the encapsulated complexes (cf. Figure 1) regarding dipole moments, dipole electric field isotropic and anisotropic polarizabilities, charges via the Mulliken, charge model 5 (CM5) and natural bond orbital (NBO) analyses are graphically presented in Figure 4 and Figure 8S of the SI and listed in Tables 2 and 11S of the SI. All used methodologies provided similar results, and those of the DFT methodologies are in good agreement with the ones obtained at the MP2/6-311 + G(d,p) and RCCSD/6-311 + G(d,p) levels for smaller systems, given in the SI.

In all cases, the isotropic polarizabilities are larger than the anisotropic ones (see Table 2). Moving from the lighter to the heavier chalcogen atoms, the polarizabilities of the capsules increase, especially for the anisotropic ones (see Table 2). Regarding the charges, (cf. Table 2 and Table 11S of SI), the replacement of the O atom with S, Se and Te in the panels results in a similar increase of the CM5 charges on the chalcogen atom. We consider that the CM5 charges, which are an extension of Hirshfeld population analysis, are the best

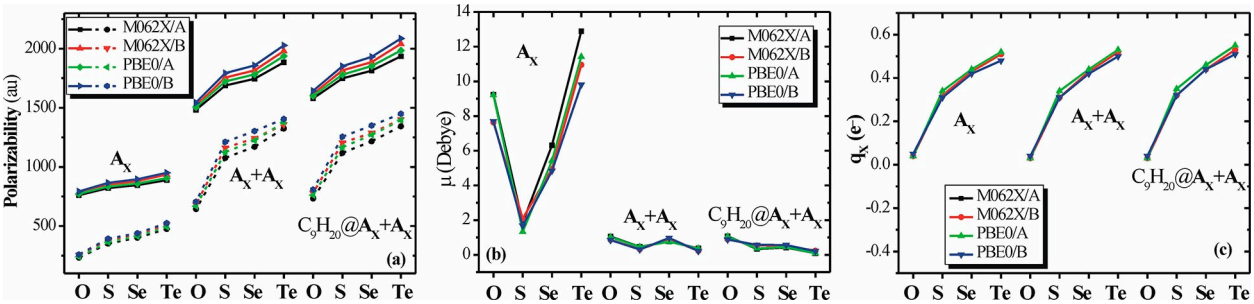

Figure 4. a) Isotropic (solid lines) and anisotropic (dotted lines) polarizabilities; b) CM5 charges qx on the chalcogen; c) Dipole moments μ of A_X, $A_X + A_X$, and C_9H_{20}@$A_X + A_X$, where X=O, S, Se and Te. [A: LANL2DZ, B: 6–311G + (d,p)].

Table 2. CM5 charges q_x on the chalcogen of A_X, dipole moments μ [Debye], dipole electric field isotropic and anisotropic polarizabilities [au], of A_X, $A_X + A_X$, C_9H_{20}@$A_X + A_X$, and C_9H_{20} molecules at M06-2X and PBE0/6-31G(d,p) level of theory.

Methods	M06-2X				PBE0			
	qx	μ	iso polar	aniso polar	q_x	μ	iso polar	aniso polar
A_O	0.04	7.629	780.09	252.28	0.05	7.695	792.28	258.92
A_S	0.32	2.096	851.65	382.01	0.31	1.677	865.03	392.21
A_{Se}	0.43	4.948	880.26	424.14	0.42	4.840	895.66	438.48
A_{Te}	0.51	10.954	934.93	511.91	0.48	9.805	949.90	524.86
$A_O + A_O$	0.03	0.866	1520.09	681.66	0.04	0.854	1543.92	705.33
$A_S + A_S$	0.31	0.319	1755.37	1161.25	0.31	0.308	1792.94	1211.30
$A_{Se} + A_{Se}$	0.43	0.906	1816.44	1242.05	0.42	0.973	1858.14	1303.03
$A_{Te} + A_{Te}$	0.52	0.227	1980.10	1358.75	0.50	0.215	2027.73	1405.53
C_9H_{20}@$A_O + A_O$	0.03	0.890	1618.71	779.14	0.04	0.879	1643.00	808.10
C_9H_{20}@$A_S + A_S$	0.32	0.543	1816.53	1204.45	0.32	0.573	1851.83	1255.03
C_9H_{20}@$A_{Se} + A_{Se}$	0.44	0.517	1886.02	1286.84	0.44	0.565	1931.15	1349.90
C_9H_{20}@$A_{Te} + A_{Te}$	0.53	0.234	2041.26	1401.95	0.51	0.206	2086.61	1449.42
C_9H_{20}		0.048	100.97	37.83		0.044	100.43	39.36

values for the calculated systems.[29] The calculated dipole moments of all capsules $\mathbf{A_X}+\mathbf{A_X}$, and encapsulation complexes $C_9H_{20}@\mathbf{A_X}+\mathbf{A_X}$ are less than 1 Debye due to the cylindrical shape of the capsules. The smallest dipole corresponds to the Te species with a value of 0.2 Debye. This is because the Te capsule and encapsulation complex are the most symmetric ones. On the contrary, for the free $\mathbf{A_X}$ cavitands, the dipole moment values decrease significantly from O to S and then it increases up to 11 Debye for the $\mathbf{A_{Te}}$ cavitand.

The ^{1}H and ^{13}C NMR spectra of the encapsulated complexes at the M06-2X/6-31G(d,p) level of theory are depicted in Figures 9S and 10S of the SI. The computed ^{1}H NMR chemical shift values of the free guest in water solution (continuum) and encapsulated in the different dimeric assemblies are shown in Figure 5. In all encapsulation complexes, $\mathbf{C_9H_{20}@A_X}+\mathbf{A_X}$, the chemical shift values of the hydrogen atoms of the guest *n*-nonane appear in the high field region of the ^{1}H NMR spectra (−2.7 to −6.3 ppm). The ^{1}H signals are upfield shifted in the encapsulation complexes in comparison of to those of free nonane in solution. The calculated proton chemical shift values for free nonane are in the range of 0.9 to 1.4 ppm. These values are in good agreement with the experimental ones (0.9 and 1.3 ppm,[30] see Figure 5). It is worth noting here that for the selenium dimer, i.e., $\mathbf{A_{Se}}+\mathbf{A_{Se}}$, the calculated chemical shifts of the hydrogen atoms of encapsulated *n*-nonane are in good agreement with those observed experimentally.[1] As previously reported for this capsular assembly,[28] the observation of larger upfield shifts for the hydrogen atoms of encapsulated nonane is a consequence of the enhanced aromaticity of its aromatic panels. As might be expected, the larger effects are observed for the central hydrogen atoms of the *n*-nonane. The largest upfield shifted chemical shift values were computed for the hydrogen atoms of nonane in the O dimer (see Figure 5 and Table 13S of SI). Nevertheless, calculations assigned to the benzofurazan wall the lower level of aromaticity in the series (see SI). This result indicates that the chemical shielding is also affected by the strong inductive effects caused by the electronegative O and N atoms. The calculated chemical shielding is affected not only by the magnetic anisotropy but also by steric and electric field effects.[31] The hydrogen atoms of the methylene groups in the middle of encapsulated nonane are involved in hydrogen bonding interactions with both N and O atoms of the aromatic walls. The average hydrogen bonding distance is close to 2.6 Å, because one of the aromatic walls of a capsular hemisphere is included in the other. In the cases of the S and Se encapsulation complexes, the methylene groups of the bound guests establish hydrogen bonds exclusively with the N atoms. For the case of Te encapsulation complex, we did not detect the formation of related hydrogen bonding interactions. The computed magnetic anisotropy of the capsule's interior provoked the calculation of different chemical shift values for germinal hydrogen atoms of the methylene groups of encapsulated nonane. i.e., the environment in the capsule is not strictly cylindrical. In the case of the O encapsulation complex, we computed the largest differences in chemical shifts in geminal hydrogen atoms. This result reflected the large deviation of the cavity's magnetic environment from a cylindrical symmetry. For both S and Se encapsulation complexes, the calculated chemical shift values for the hydrogen atoms of bound nonane are similar, see Figure 5. We explain this finding due to the formation of similar HCH···N hydrogen bonding interactions in the two complexes. On the other hand, the encapsulation complex of the Te capsule, in which the two cavitands defining the two hemispheres are strongly bonded, displays a cavity of cylindrical symmetry. For this reason, we observed small deviations in the computed chemical shift value of geminal hydrogen atoms even in different methylene groups of alkyl chain of the bound nonane. Thus, the shape of the curve delimited by the calculated chemical shifts for the different hydrogen atoms (Figure 5) resembles the straight line obtained in the analogous plot of calculated chemical shifts of the hydrogen atoms for the alkane free in solution.

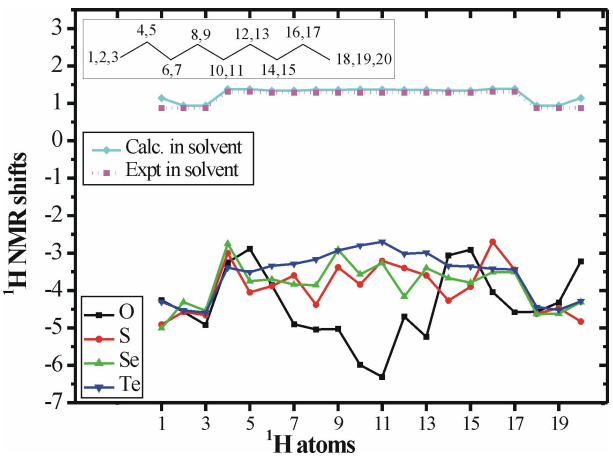

Figure 5. ^{1}H NMR shifts [ppm] of the n-C9H20 compound encapsulated and in solvent at M06-2X/6-31G(d,p) level of theory.

Contours of the magnetic isotropy and anisotropy values of the capsules $\mathbf{A_X}+\mathbf{A_X}$ and their encapsulation complexes $\mathbf{C_9H_{20}@A_X}+\mathbf{A_X}$, where X=O, S, Se and Te, on the XY plane perpendicular to the main Z axis of the capsule and at distances R=0–8 Å from the center of mass of the capsule along the same axis are depicted in Figure 6 (for R=0 and 4 or 2 Å). Figs 11S-14S of SI (for R=0–8 Å). Similarly, the computed Nucleus-Independent Chemical Shift values (NICS) aromaticity indexes are depicted in Figs 15S–16S of the SI.

It is interesting to note that the empty capsules $\mathbf{A_X}+\mathbf{A_X}$ and their encapsulation complexes $\mathbf{C_9H_{20}@A_X}+\mathbf{A_X}$, present unusually high magnetic anisotropy values. Moreover, the magnitude of the anisotropic magnetic component is equal to the isotropic counterpart, Figs 15S-16S of the SI. In most of the empty $\mathbf{A_X}+\mathbf{A_X}$ capsules, the plot of the XY plane at R=0, beautifully reflects the empty space of the cavity. However, this is not the cases for the O capsule. We already mentioned above that in the empty dimer of the O cavitands one aromatic wall of one hemisphere is included in the other. In similar plots of the magnetic components of chemical shielding for the encapsulation complexes $\mathbf{C_9H_{20}@A_X}+\mathbf{A_X}$, the alkane can clearly be observed. For Te encapsulation complex, the alkane appears in the middle of the plots of the XY planes because it is encapsulated along

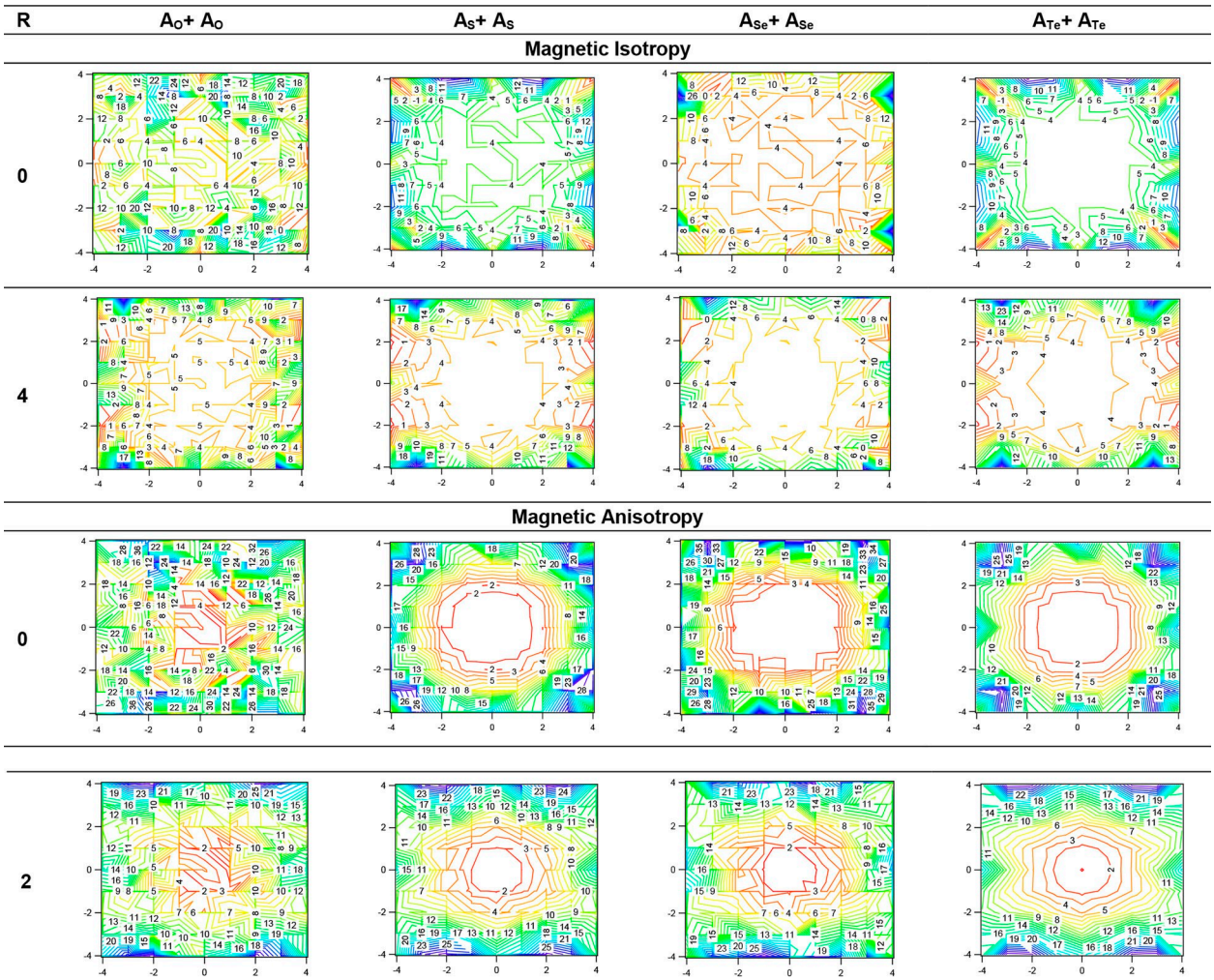

Figure 6. Contours of the magnetic isotropy and anisotropy values of $A_X + A_X$ capsules, where X=O, S, Se and Te, on the XY plane perpendicular to the main Z axis and at distances R along the same axis from the center of the capsule.

the Z axis. In contrast, for the S and Se encapsulation complexes, the alkane is not encapsulated along the Z-axis of the capsule. The encapsulated alkane interacts with the walls of the capsule appearing moved away from the center of the plots of the XY planes, see Figure 1. Remarkably, in some areas of the XY planes the magnetic anisotropy component is larger than the isotropic counterpart.

Some similarities can be drawn by comparing the plots of the chemical shielding components of the different capsules and their encapsulation complexes. The assemblies based on S and Se atoms present similarities regarding the shape of the contours of the magnetic isotropy and anisotropy components. For the assemblies containing the Te atom, we observe similarities with respect to the shapes of the contour plots of the isotropic component with those of the S and Se analogues at distances of 4–8 Å along the Z axis. This observation indicates that after 4 Å, the effect of the high polarizability of the Te chalcogen diminishes. In relation to the contour plots of the anisotropy component, those of Te assemblies are similar at all distances to that of the S and Se counterparts. At distances of 2–3 Å along the main Z axis, the magnetic anisotropy values are the largest ones at the central areas of the XY planes, see Figure 6. For the encapsulation complexes $\mathbf{C_9H_{20}@A_X + A_X}$, the four chalcogen atom result in a similar chemical shielding effect at distances of 7–8 Å. This result indicates that at distances larger than 7 Å, the chalcogen atom has no effect on the computed shielding.

The NICS index is widely used to characterize aromaticity and antiaromaticity of molecular systems[32] and it is relatively insensitive to the level of theory used for its calculation (basis set and method).[25] The computed NICS value at certain points can be used to characterize the shielding environment produced by a molecule at the defined point. More negative NICS indexes correspond to an enhanced aromaticity, while positive values indicate antiaromaticity. Not surprisingly, for the empty $\mathbf{A_X + A_X}$ capsules, the contour plots of the NICS values in the XY planes at distances of 0–2 and 7–8 Å from the center of mass of the assemblies are different for the O assembly compared to those of the other three chalcogen atoms. The dimensions of *n*-nonane are 1.8×2.2×12.0 Å. In the empty

capsules, the NICS indexes at positions occupied by the hydrogen atoms of the alkane in the encapsulation complexes are in the range of −4 to −6. The magnitude of the computed values correspond to NICS values at the center of common aromatic rings, i.e., NICS(0) of phenalene, oxo-and/or aza-phenalene.[33] The calculation of the NICS values at the same locations in the encapsulation complexes revealed an increase in the negative NICS values, see NICS contour plots Figure 16S of SI.

4. Summary and Conclusions

We computed the molecular structures of dimeric capsules stabilized by chalcogen bonding and their encapsulation complexes with *n*-nonane, as well as, the chemical shielding exerted by the capsule's aromatic walls in their empty cavities and in the hydrogen atoms of the encapsulated guest. The calculated binding energies of the more stable empty capsules are −1.4(O) −1.5(S), −1.8(S) and −4.6 eV (Te). The energetic penalty for the arrangement of the aromatic walls in a non-planar orientation (structure b of the empty capsules) is quantified as 2.5 eV for the Te derivative and 0.2 eV for the Se analogue. On the other hand, for the S derivative, the non-planar arrangement of the aromatic walls resulted to be slightly lower in energy (0.1 eV). For the O derivative, the arrangement of the aromatic panels in a planar geometry favoring an array of chalcogen bonding interactions turned out not be an energy minimum. The binding energies of $C_9H_{20}@\mathbf{A_X}+\mathbf{A_X}$, with respect to the three components of the encapsulated species, range for −1.9 (O) to −5.3 (Te) eV. The calculated energy differences are in the range of −1.9 (O) to −5.3 (Te) eV. Via many-body analyses we found that the interaction of the three components in the $C_9H_{20}@\mathbf{A_X}+\mathbf{A_X}$, i.e., 3-body term, further stabilizes the encapsulated complexes.

The calculated chemical shift values for the hydrogen atoms of encapsulated *n*-nonane are significantly upfield shifted with respect to those computed for the free guest. The magnitudes of the chemical shifts calculated for encapsulated nonane in the Se capsule and free nonane[30] nicely agree with those observed in the experimental ^{1}H NMR spectrum of the assembly.[1] The hydrogen atoms of the encapsulated nonane in the S-, Se- and Te-chalcogen bonded capsules display larger experimental and calculated upfield shifts than those observed for the guest bound in hydrogen bonded counterparts.[1] We conclude that this effect is a direct consequence of the enhanced aromaticity of the walls of the chalcogen-bonded capsules. It is worthy to note here that NICS values inside the chalcogen-bonded capsules and at the position occupied by the hydrogen atoms of the alkane are similar to the NICS values inside common aromatic rings such as phenalene, oxo-and/or aza- phenalene. The larger differences in chemical shift values for the hydrogen atoms of nonane encapsulated in chalcogen and hydrogen-bonded capsules is observed and computed for the central methylene groups in the alkyl chain of the guest. For the encapsulation complex of the O capsule, the large upfield chemical shifts observed and computed for the hydrogen atoms of the bound guests are also attributed to an increase of the chemical shielding provided by the aromatic cavity. However, in this case the main responsible are the inductive effects caused by the electronegative O and N atoms, i.e., the electric field effects.

The interiors of all capsules, $\mathbf{A_X}+\mathbf{A_X}$, and their encapsulation complexes $C_9H_{20}@A_X+\mathbf{A_X}$ display similar values of the two components of chemical shielding: isotropic and the anistropic. Remarkably, the calculated values for the anisotropic component are unusually high. For the Te capsule, its large chemical shielding mainly derives from the large polarizability of the Te atom. In contrast, for the O and N derivatives, the inductive effects exerted by the electronegative O and N atoms and the interactions that they establish with other atoms provoke the increase in chemical shielding. Finally, for the S and Se capsules, the increase in chemical shielding results from a combination of the large polarizability of the S and Se atoms and the electric field effects deriving from their noticeable electronegativity. Supramolecular capsules are known to stabilize reactive intermediates and unstable species. The putative encapsulation of molecular magnets might be sensible to the magnetic environment of the capsules' interior.

Experimentally, dimeric capsules containing sulfur, selenium and tellurium 1,3-diazole units (X=S, Se, and Te) were synthesized. Based on recent experimental evidence of chalcogen bonding involving oxygen acceptor atoms, we examined, from a theoretical point of view the possibility of assembling analogous capsules equipped with oxygen containing 1–3-diazole units (benzofurazan). The results of our theoretical calculations predict that in the case of O derivatives as capsules' hemispheres, the aromatic wall of one of the hemispheres is selectively included in the cavity of the other hemisphere. The resulting dimeric assembly is stabilized through π–π stacking inclusion featuring a collapsed aromatic cavity. For this reason, the encapsulation of the nonane into the $\mathbf{A_O}+\mathbf{A_O}$ dimer is not energetically favorable. Nevertheless, the encapsulation complex, $C_9H_{20}@\mathbf{A_O}+\mathbf{A_O}$, displays a structure that is an energy minimum, The $C_9H_{20}@\mathbf{A_O}+\mathbf{A_O}$ complex is stabilized by π–π stacking interactions, hydrogen bonds formed between *n*-nonane and the heteroatoms of the cavitands, and additional CH-π interactions.

Supporting Information

Geometries, many body analysis of the binding energies, dipole moments, charges on the chalcogen, dipole electric field isotropic and anisotropic electric field polarizabilities, ^{1}H and ^{13}C NMR spectra, contour plots of magnetic isotropy and anisotropy and NICS indexes of $\mathbf{A_X}+\mathbf{A_X}$ and $C_9H_{20}@\mathbf{A_X}+\mathbf{A_X}$ at different levels of theory.

Acknowledgments

We acknowledge support of this work by the projects: i) "Advanced Materials and Devices" (MIS 5002409) which is implemented under

the "Action for the Strategic Development on the Research and Technological Sector" and ii) "National Infrastructure in Nanotechnology, Advanced Materials and Micro- / Nanoelectronics" (MIS 5002772) which is implemented under the Action "Reinforcement of the Research and Innovation Infrastructure", funded by the Operational Programme "Competitiveness, Entrepreneur-ship and Innovation" (NSRF 2014–2020) and co-financed by Greece and the European Union (European Regional Development Fund).

Conflict of Interest

The authors declare no conflict of interest.

Keywords: capsules · cavitands · chalcogen bonding · density functional calculations · magnetic anisotropy · molecular recognition

[1] F.-U. Rahman, D. Tzeli, I. D. Petsalakis, G. Theodorakopoulos, P. Ballester, J. Rebek Jr., Y. Yu, *J. Am. Chem. Soc.* **2020**, *142*, 5876–5883.
[2] L. J. Riwar, N. Trapp, K. Root, R. Zenobi, F. Diederich, *Angew. Chem. Int. Ed.* **2018**, *57*, 17259–17264.
[3] M. D. Pluth, R. G. Bergman, K. N. Raymond, *Acc. Chem. Res.* **2009**, *42*, 1650–9.
[4] C. L. Gibb, B. C. Gibb, *J. Am. Chem. Soc.* **2004**, *126*, 11408–11409.
[5] K. Wang, X. Cai, W. Yao, D. Tang, R. Kataria, H. S. Ashbaugh, L. D. Byers, B. C. Gibb, *J. Am. Chem. Soc.* **2019**, *141*, 6740–6747.
[6] Z. Q. Tiefenbacher, L. Catti, K. Tiefenbacher, *Acc. Chem. Res.* **2018**, *51*, 2107–2114.
[7] K. Eichstaedt, A. Wasilewska, B. Wicher, M. Gdaniec, T. Połoński, *Cryst. Growth Des.* **2016**, *16*, 1282–1293.
[8] B. D. Lindner, B. A. Coombs, M. Schaffroth, J. U. Engelhart, O. Tverskoy, F. Rominger, M. Hamburger, U. H. Bunz, *Org. Lett.* **2013**, *15*, 666–669.
[9] J. Lee, L. M. Lee, Z. Arnott, H. Jenkins, J. F. Britten, I. Vargas-Baca, *New J. Chem.* **2018**, *42*, 10555–10562.
[10] A. F. Cozzolino, G. Dimopoulos-Italiano, L. M. Lee, I. Vargas-Baca, *Eur. J. Inorg. Chem.* **2013**, 2751–2756.
[11] D. J. Pascoe, K. B. Ling, S. L. Cockroft, *J. Am. Chem. Soc.* **2017**, *139*, 15160–15167.
[12] G. E. Garrett, G. L. Gibson, R. N. Straus, D. S. Seferos, M. S. Taylor, *J. Am. Chem. Soc.* **2015**, *137*, 4126–4133.
[13] A. F. Cozzolino, I. Vargas-Baca, S. Mansour, A. H. Mahmoudkhani, *J. Am. Chem. Soc.* **2005**, *127*, 3184–3190.
[14] T. Fellowes, B. L. Harris, J. M. White, *Chem. Commun.*, **2020**, *56*, 3313–3316.
[15] K. T. Mahmudov, M. N. Kopylovich, M. F. C. Guedes da Silva, A. J. L. Pombeiro, *Dalton Trans.*, **2017**, *46*, 10121–10138.
[16] a) Y. Zhao, D. G. Truhlar, *Theor. Chem. Acc.* **2008**, *120*, 215–241; b) Y. Zhao, D. G. Truhlar, *Acc. Chem. Res.* **2008**, *41*, 157–167.
[17] a) P. J. Hay, W. R. Wadt, *J. Chem. Phys.* **1985**, *82*, 299–310; b) L. E. Roy, P. J. Hay, R. L. Martin, *J. Chem. Theory Comput.* **2008**, *4*, 1029–1031.
[18] a) P. C. Hariharan, J. A. Pople, *Theor. Chim. Acta* **1973**, *28*, 213–222; b) M. M. Francl, W. J. Petro, W. J. Hehre, J. S. Binkley, M. S. Gordon, D. J. DeFrees, J. A. Pople, *J. Chem. Phys.* **1982**, *77*, 3654–3665; c) V. Rassolov, J. A. Pople, M. Ratnerand, T. L. Windus, *J. Chem. Phys.* **1988**, *109*, 1223–1229.
[19] a) J. P. Perdew, K. Burke, M. Ernzerhof, *Phys. Rev. Lett.* **1996**, *77*, 3865–3868; b) M. Enzerhof, G. E. Scuseria, *J. Chem. Phys.* **1999**, *110*, 5029–5036; c) C. Adamo, V. Barone, *J. Chem. Phys.* **1999**, *110*, 6158–6170.
[20] D. Tzeli, I. D. Petsalakis, G. Theodorakopoulos, *Chem. Phys. Lett.* **2013**, *573*, 48–55.
[21] S. F. Boys, F. Bernardi, *Mol. Phys.* **1970**, *19*, 553–566.
[22] D. Hankins, J. W. Moskowitz, F. H. Stillinger, *J. Chem. Phys.* **1970**, *53*, 4544–4554.
[23] D. Tzeli, A. Mavridis, S. S. Xantheas, *J. Phys. Chem. A* **2002**, *106*, 11327–11337.
[24] a) F. London, *J. Phys. Radium*, **1937**, *8*, 397–409; b) J. R. Cheeseman, G. W. Trucks, T. A. Keith, M. J. A. Frisch, *J. Chem. Phys.* **1996**, *104*, 5497–509.
[25] Z. Chen, C. S. Wannere, C. Corminboeuf, R. Puchta, P. R. Schleyer, *Chem. Rev.* **2005**, *105*, 3842–3888.
[26] Gaussian 16, Revision C.01, M. J. Frisch, G. W. Trucks, H. B. Schlegel, G. E. Scuseria, M. A. Robb, J. R. Cheeseman, G. Scalmani, V. Barone, G. A. Petersson, H. Nakatsuji, X. Li, M. Caricato, A. V. Marenich, J. Bloino, B. G. Janesko, R. Gomperts, B. Mennucci, H. P. Hratchian, J. V. Ortiz, A. F. Izmaylov, J. L. Sonnenberg, D. Williams-Young, F. Ding, F. Lipparini, F. Egidi, J. Goings, B. Peng, A. Petrone, T. Henderson, D. Ranasinghe, V. G. Zakrzewski, J. Gao, N. Rega, G. Zheng, W. Liang, M. Hada, M. Ehara, K. Toyota, R. Fukuda, J. Hasegawa, M. Ishida, T. Nakajima, Y. Honda, O. Kitao, H. Nakai, T. Vreven, K. Throssell, J. A. Montgomery, Jr., J. E. Peralta, F. Ogliaro, M. J. Bearpark, J. J. Heyd, E. N. Brothers, K. N. Kudin, V. N. Staroverov, T. A. Keith, R. Kobayashi, J. Normand, K. Raghavachari, A. P. Rendell, J. C. Burant, S. S. Iyengar, J. Tomasi, M. Cossi, J. M. Millam, M. Klene, C. Adamo, R. Cammi, J. W. Ochterski, R. L. Martin, K. Morokuma, O. Farkas, J. B. Foresman, D. J. Fox, Gaussian, Inc., Wallingford CT, **2016**.
[27] C. Janiak, *J. Chem. Soc. Dalton Trans.*, **2000**, 3885–3896.
[28] D. Tzeli, I. D. Petsalakis, G. Theodorakopoulos, *Phys. Chem. Chem. Phys.*, **2011**, *13*, 11965–11975.
[29] A. V. Marenich, S. V. Jerome, C. J. Cramer, D. G. Truhlar, *J. Chem. Theory Comput.* **2012**, *8*, 527–541.
[30] H NMR: http://www.molbase.com/en/hnmr_111-84-2-moldata-73715.html.
[31] M. Baranac-Stojanović, *RSC Adv.* **2014**, *4*, 308—321.
[32] A. Stranger, *J. Org. Chem.* **2006**, *71*, 883–893.
[33] D. Tzeli, P. Kozielewicz, M. Zloh, D. Antonow, P. Tsoungas, I. D. Petsalakis, *ChemistrySelect* **2018**, *3*, 9743–9752.

Manuscript received: July 27, 2020
Accepted manuscript online: July 29, 2020
Version of record online: September 1, 2020